Letters

A Frequency-Based Stray Parameter Extraction Method Based on Oscillation in SiC MOSFET Dynamics

Sideng Hu, *Member, IEEE*, Mingyang Wang, Zipeng Liang, and Xiangning He, *Fellow, IEEE*

***Abstract*—The dynamic switching procedure of an SiC device is highly related to the circuit stray parameters. Based on that fact, a specific extraction platform with SiC MOSFET is presented as the extraction tool and works independently with the converter topology. The stray inductance for the arbitrary power flow path in the converter can be experimentally extracted. As only the voltage oscillation in SiC MOSFET dynamics is measured, the uncertainty and errors in the previous time-domain methods caused by the probes synchronization, integral time zone selection, and voltage offset from a parasitic resistor get eliminated. Meanwhile, through the extension of the equivalent circuit equations, this method is also available in the stray capacitance extraction. Experimental results in the copper and laminated bus bars for the large-capacity converters validate the feasibility of the proposed method.**

***Index Terms*—Bus bar, extraction, oscillation, SiC MOSFET, stray parameter.**

I. Introduction

In POWER electronic systems, the extraction of the stray parameters is essential for the design and optimization of bus bars [1], [2]. Previous research works on the extraction methods can be clarified into three categories: finite element method (FEM) software calculation, professional equipment (high precision *LCR* meter or impedance analyzer), and experimental testing [3]. In FEM calculation, the stray parameters are calculated based on the field equations with the numerical algorithm [4]. Due to the complexity in modeling and calculation, it mainly focuses on the large size components but the effect from environment interference and detailed structure in a real system is often ignored. For professional equipment methods, the high-precision *LCR* meter and impedance analyzer are used for the stray parameters' measurement. It suffers from the cost and time-cost correction work to ensure the accuracy due to the placement and errors from the clip [5].

Manuscript received August 23, 2020; revised September 28, 2020; accepted October 19, 2020. Date of publication October 26, 2020; date of current version February 5, 2021. This work was supported in part by the National Natural Science Foundation of China under Grant 51777188 and in part by the Power Electronics Science and Education Development Program of Delta Environmental & Educational Foundation under Grant DREG2019019. *(Corresponding author: Sideng Hu.)*

The authors are with the College of Electrical Engineering, Zhejiang University, Hangzhou 310058, China (e-mail: husideng@zju.edu.cn; 21810197@zju.edu.cn; loavigil@163.com; hxn@zju.edu.cn).

Color versions of one or more of the figures in this letter are available online at https://ieeexplore.ieee.org.

Digital Object Identifier 10.1109/TPEL.2020.3033801

Other than the above-mentioned methods, the experimental testing is developed based on the dynamic behavior of switching devices, which is named the time-domain method (TDM) [3], [6], [7]. The stray inductance is calculated based on the formula $U = L(di/dt)$, where the voltage U and current slope di/dt are measured during the switching process. The accuracy of TDM is highly related to the voltage and current probes for capturing the nanosecond waveforms. Meanwhile, the advanced data process method is also important to improve the extraction accuracy from the nonideal waveforms [7]. To overcome the limitations in the conventional TDM, a frequency-domain method (FDM) has been studied [8], [9]. The underdamped oscillation frequency and its relation with the loop's parameters in a device-related power flow path are utilized. Existing TDM and FDM mainly focus on the stray inductance but the effect of the stray capacitance on accuracy is still unclear [10]. Meanwhile, both methods take use of the converter bridge for the pulse generation. First, the switching rate is limited, especially for the insulated gate bipolar translator (IGBT) in a high-power converter. The tail current effect also trends to dissipate the energy stored in the stray inductance. Thus, the high-frequency oscillation is hard to be triggered and captured. Second, the value of total parameters in the device-related loop can be obtained, but the extension for the individual components in the loop or dc-link conductor for connecting the multiple converters is hard to achieve.

For solving the above-mentioned problems, this letter proposed a novel frequency-based stray parameter extraction method based on the oscillation in SiC MOSFET dynamics. The stray inductance and capacitance for the arbitrary power flow loop in the converter can be experimentally extracted. Its effect gets verified by the experimental results on the power loop formed by the laminated and copper bus bars. A fully automated extraction procedure is also presented for other applications.

II. Principle of Stray Parameter Extraction Based on Switching Procedure

The conventional TDMs take use of the half-bridge unit in a converter for the pulse generation, as presented in Fig. 1(a). By testing the dynamic waveforms of V_{ce}, V_D, and I_{ce} in a switching procedure, the stray inductance L_s can be extracted as

$$L_s = \int_{t_1}^{t_2} [V_{\rm dc} - V_{ce}(t) - V_D(t)]\, dt / [I_{ce}(t_1) - I_{ce}(t_2)]. \quad (1)$$

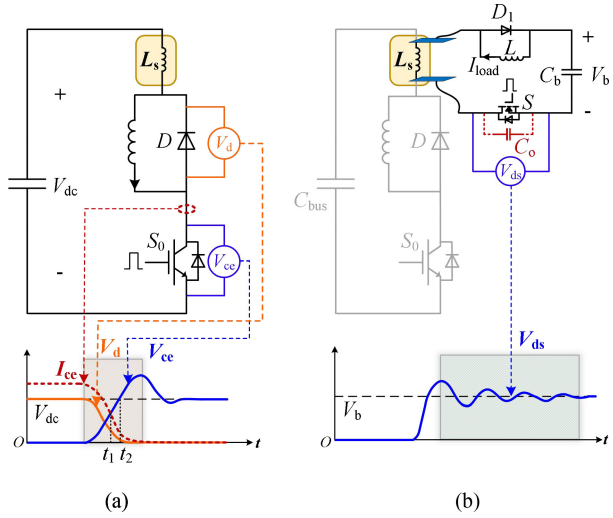

Fig. 1. Stray parameter extraction platform and waveform tested region for the bus bar. (a) TDM embedded in the convertor. (b) Proposed frequency-based method outside the convertor.

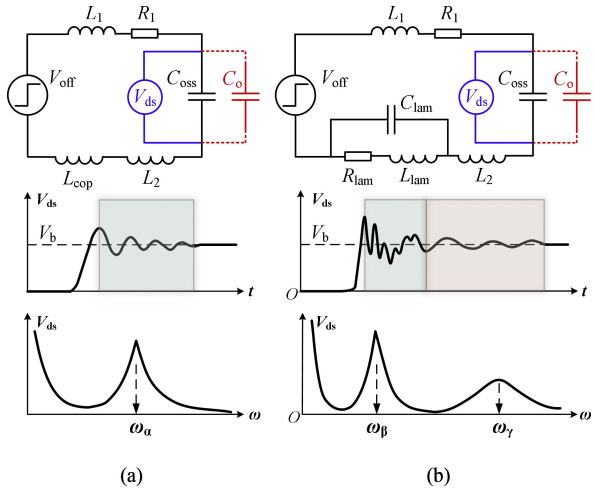

Fig. 2. Equivalent circuit and switching characteristic of $V_{\rm ds}$. (a) Inductance-dominated bus bar. (b) Capacitance-included bus bar.

The accuracy in the conventional TDMs is related to the measurement of items in (1) and is easily affected by the factors as follows:

1) bandwidth difference and synchronization problem between the voltage and current probes;
2) voltage measurement error from the offset in probes and distribution on the parasitic resistor;
3) integral time zone selection (t_1–t_2) in the nonideal switching transient;

In Fig. 1(b), the ringing oscillation triggered by the turn-off procedure of SiC MOSFET is utilized for the stray parameter extraction. Fig. 2 presents the equivalent circuits during the oscillation [11]. Fig. 2(a) shows the situation in the inductance-dominated application, such as copper bus bar. Fig. 2(b) shows the situation for the stray capacitance included application, such as the laminated bus bar. The L_1 and R_1 mean the stray inductor and parasitic resistor in the extraction platform and $V_{\rm off}$ means the step excitation source. Additional $C_{\rm o}$ is added as a parallel capacitor on SiC MOSFET for frequency adjustment. Compared with the conventional TDM in Fig. 1(a), first, only drain–source voltage $V_{\rm ds}$ is measured. Thus, the wide bandwidth current probes requirement and synchronization issues with the voltage probes get avoided. Second, as only the oscillation frequency is required, the uncertainty caused by the time zone selection and parasitic resistor is also eliminated.

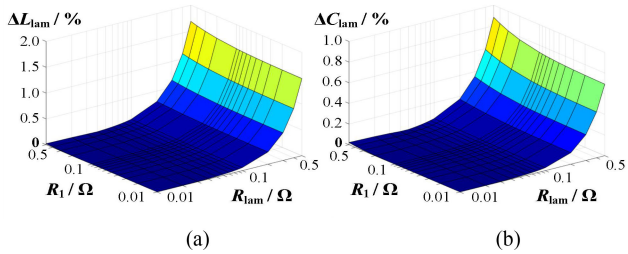

Fig. 3. Relative error of stray parameters extraction in a laminated bus bar. (a) Stray inductance. (b) Stray capacitance.

A. *Extraction Principle for Inductance-Dominated Application*

The copper bus bar is widely adopted as the dc-link connector for the multiple converters and the large-capacity converters. Fig. 2(a) shows the equivalent circuit with $V_{\rm ds}$ oscillation and $L_{\rm cop}$ represents the stray inductor in the tested copper bus bar. Let L_{12} equal to the sum of L_1 and L_2. The L_2 means the additional inductance from the conductor between the tested target and platform. Due to the lack of a stacked area between the positive and negative bus bar, the stray capacitor in the copper bus bar is often ignored.

From the oscillation triggered by the turn-off procedure of SiC MOSFET, the oscillation frequency ω observed in $V_{\rm ds}$ satisfies the formula of underdamped oscillation in the second-order *RLC* circuit, as presented

$$\omega = \sqrt{\frac{1}{(L_{12}+L_{\rm cop})C_{\rm oss}} - \frac{R_1^2}{4(L_{12}+L_{\rm cop})^2}}. \tag{2}$$

For an unknown $C_{\rm oss}$, two steps, including capturing the oscillation without and with additional C_o, are required. The corresponding frequencies are recorded as $\omega_{\alpha 1}$ and $\omega_{\alpha 2}$. For a given $C_{\rm oss}$ from the datasheet, the step with C_o can be passed in rough extraction. The sum of L_{12} and $L_{\rm cop}$ is then be calculated by solving formula (3). The inductance L_{12} can be obtained and excluded by an additional test with only L_2 embedded in the extraction platform.

$$\begin{cases} 1 = \omega_{\alpha 1}^2 (L_{12}+L_{\rm cop})C_{\rm oss} \\ 1 = \omega_{\alpha 2}^2 (L_{12}+L_{\rm cop})(C_{\rm oss}+C_o). \end{cases} \tag{3}$$

The resistance-related item is set to zero due to the relatively small R_1 and its effect is discussed in Fig. 3.

TABLE I
INDUCTANCE AND CAPACITANCE PARAMETERS FOR SIMULATION

Variable	Description	Value
$L_{\rm lam}$	Tested inductance in laminated bus bar (nH)	40
$C_{\rm lam}$	Tested capacitance in laminated bus bar (nF)	5
L_{12}	Sum of extract inductance in tested loop (nH)	60
$C_{\rm oss}$	Output capacitance of SiC MOSFET (pF)	120
$C_{\rm o}$	Added output capacitance (pF)	220

B. Extension for the Stray Capacitance-Included Application

The laminated bus bar is widely used for the device voltage stress depression purpose. It features in a low stray inductance benefits with a significant capacitance. The stray inductance extraction should thereby be researched with the capacitor effect. As shown in Fig. 2(b), the lumped stray capacitor $C_{\rm lam}$ and resistor $R_{\rm lam}$ are included. The equivalent model turns to be a fourth-order circuit and the step response transfer function for $V_{\rm ds}$ is presented in the following equation, where $L_{\rm lam}$ means the stray inductance from the tested laminated bus bar

$$G(s) = V_{\rm dc}\frac{C_{\rm lam}L_{\rm lam}s^2 + C_{\rm lam}R_{\rm lam}s + 1}{s(K_1s^4 + K_2s^3 + K_3s^2 + K_4s^1 + 1)}$$

$$\begin{cases} K_1 = C_{\rm lam}(C_{\rm oss}{+}C_o)L_{\rm lam}L_{12} \\ K_2 = C_{\rm lam}(C_{\rm oss}{+}C_o)(L_{\rm lam}R_1 + L_{12}R_{\rm lam}) \\ K_3 = C_{\rm lam}(C_{\rm oss}{+}C_o)R_1R_{\rm lam} + C_{\rm lam}L_{\rm lam} \\ \qquad +(C_{\rm oss}{+}C_o)(L_{12} + L_{\rm lam}) \\ K_4 = C_{\rm lam}R_{\rm lam} + (C_{\rm oss}{+}C_o)(R_1 + R_{\rm lam}). \end{cases} \tag{4}$$

Two pairs of conjugate complex poles can be observed in (4) and that indicate the observed underdamped oscillation contains two frequencies, as shown in Fig. 2(b). Two steps are then performed as capturing the oscillations without and with additional C_o. The corresponding frequencies are obtained by the fast Fourier transform (FFT) and recorded as $\omega_{\beta 1}$, $\omega_{\gamma 1}$, and $\omega_{\beta 2}$, $\omega_{\gamma 2}$. The equations with the four frequencies are formed as given in (5). The results of $L_{\rm lam}$, $C_{\rm lam}$, L_{12}, and $C_{\rm oss}$ can be extracted through solving the equations as

$$\begin{cases} 1 = \omega_{\beta 1}^2\left[C_{\rm lam}L_{\rm lam} + C_{\rm oss}(L_{\rm lam} + L_{12})\right] \\ \quad -\omega_{\beta 1}^4 C_{\rm lam}C_{\rm oss}L_{\rm lam}L_{12} \\ 1 = \omega_{\gamma 1}^2\left[C_{\rm lam}L_{\rm lam} + C_{\rm oss}(L_{\rm lam} + L_{12})\right] \\ \quad -\omega_{\gamma 1}^4 C_{\rm lam}C_{\rm oss}L_{\rm lam}L_{12} \\ 1 = \omega_{\beta 2}^2\left[C_{\rm lam}L_{\rm lam} + (C_{\rm oss}{+}C_o)(L_{\rm lam} + L_{12})\right] \\ \quad -\omega_{\beta 2}^4 C_{\rm lam}(C_{\rm oss}{+}C_o)L_{\rm lam}L_{12} \\ 1 = \omega_{\gamma 2}^2\left[C_{\rm lam}L_{\rm lam} + (C_{\rm oss}{+}C_o)(L_{\rm lam} + L_{12})\right] \\ \quad -\omega_{\gamma 2}^4 C_{\rm lam}(C_{\rm oss}{+}C_o)L_{\rm lam}L_{12}. \end{cases} \tag{5}$$

The influence of R_1 and $R_{\rm lam}$ on the stray parameter extraction is analyzed with the parameters in Table I. According to the imaginary part of poles in (4), the relative errors in $L_{\rm lam}$ and $C_{\rm lam}$ are calculated from (5) and shown in Fig. 3. It can be found that the relative error is under 2%, thus a high accuracy gets ensured without the consideration of the parasitic resistor.

Based on the analysis mentioned above, the flowchart of the proposed stray parameter extraction method is presented in Fig. 4. It includes frequencies extraction and equations solving, which are both programmable and can be executed automatically.

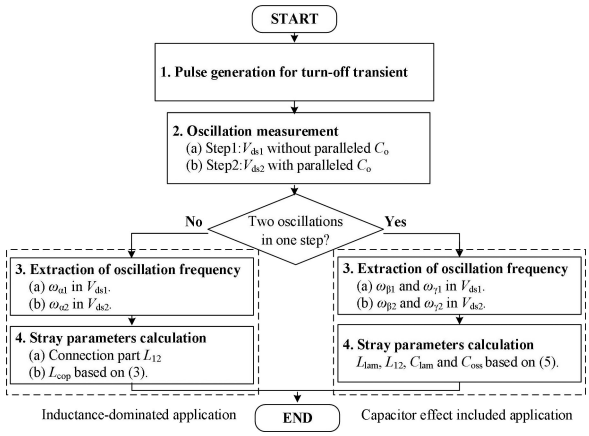

Fig. 4. Flowchart of the proposed stray parameters extraction method.

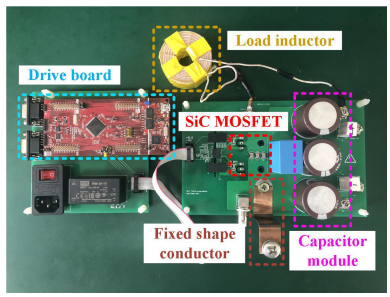

Fig. 5. Diagram of the compact stray parameters extraction platform.

III. EXPERIMENTAL VALIDATION

A stray parameters extraction platform with SiC MOSFET (C2M0040120) is shown in Fig. 5. The fixed shape conductor L_2 is connected to the tested target and is flexible to satisfy the shape of the power flow path in different tested bus bars. The impedance analyzer (WK65120B) is taken for verification. Considering the test error, a sophisticated clip placement work is carried and aims to provide a reference for the comparison.

A. Comparison Study Between the Time-Domain and Frequency-Based Method.

The stray inductance L_1 in the extraction platform is measured by the TDM based on formula (1) and the proposed frequency-based method. In formula (1), V_{ce} and I_{ce} are replaced by $V_{\rm ds}$ and $I_{\rm ds}$ for the application of SiC MOSFET. Fig. 6 illustrates the dynamic waveforms in testing. The extraction results of L_1 by the time-domain and frequency-based method are listed in Table II.

Compared with the TDM, the frequency-based method holds a higher extraction accuracy with no more than 5% relative error and higher stability in a different time zone selection. It mainly results from the solved probes synchronization issues and voltage offset from the parasitic resistor.

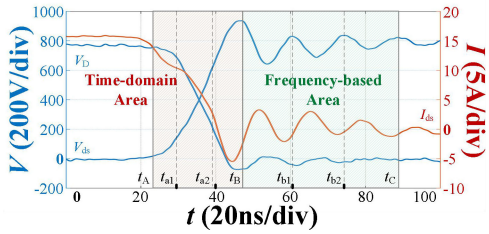

Fig. 6. Dynamic waveforms of SiC MOSFET in L_1 extraction.

TABLE II
RESULTS COMPARISON WITH DIFFERENT EXTRACTION METHODS

Method	Time zone	L_1	Relative error
Impedance Analyzer (IM3570)	/	43.1 nH	/
Time-domain Method	t_A-t_{a1}	24.1 nH	44.1 %
	t_{a1}-t_{a2}	27.1 nH	37.1 %
	t_{a2}-t_B	33.1 nH	23.2 %
Frequency-based Method	t_B-t_{b1}	41.2 nH	4.4 %
	t_{b1}-t_{b2}	41.3 nH	4.2 %
	t_{b2}-t_C	41.8 nH	3.0 %

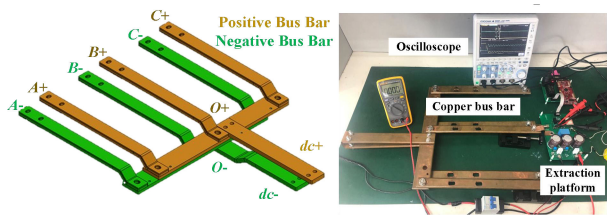

(a) (b)

Fig. 7. Parameter extraction of the copper bus bar. (a) Geometry structure. (b) Experimental platform.

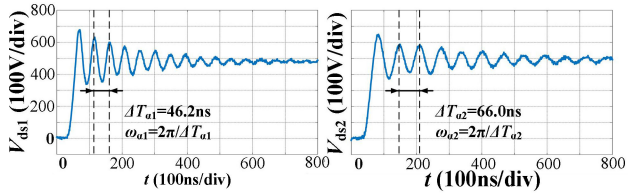

(a) (b)

Fig. 8. Experimental waveforms of V_{ds} for the copper bus bar. (a) V_{ds1} without C_o. (b) V_{ds2} with C_o.

B. Extraction in Inductance-Dominated Copper Bus Bar

A copper bus bar from the dc link in a three-phase inverter is tested, as shown in Fig. 7. The stray parameters from the A_+, B_+, and C_+ to the three-phase terminals A_-, B_-, and C_- are tested in Fig. 7(b). In the extraction platform, the bus voltage V_b is set to 500 V with 10 A I_{load} and C_o is selected as 150 pF.

The oscillation waveforms of V_{ds} are shown in Fig. 8 with the oscillation frequencies $\omega_{\alpha1}$ and $\omega_{\alpha2}$ calculated from $\Delta T_{\alpha1}$ and $\Delta T_{\alpha2}$. According to formula (3), L_{12} is extracted as 125 nH. The calculation results of the tested copper bus bar L_{cop} are presented in Table III compared with the results from the impedance analyzer. The proposed method is capable of a copper bus bar with a 3% relative error.

TABLE III
EXPERIMENTAL AND IMPEDANCE ANALYZER RESULT OF COPPER BUS BAR

Section	Experiment	Impedance analyzer	Relative error
A_+ to A_-	249 nH	241 nH	3.0 %
B_+ to B_-	159 nH	164 nH	2.7 %
C_+ to C_-	201 nH	208 nH	3.1 %

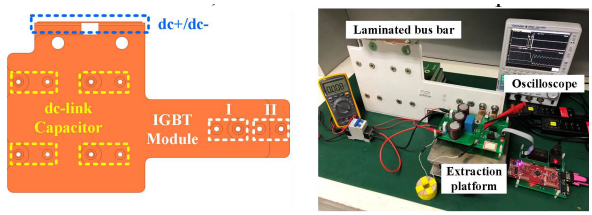

(a) (b)

Fig. 9. Parameter extraction of the laminated bus bar. (a) Geometry structure. (b) Experimental platform.

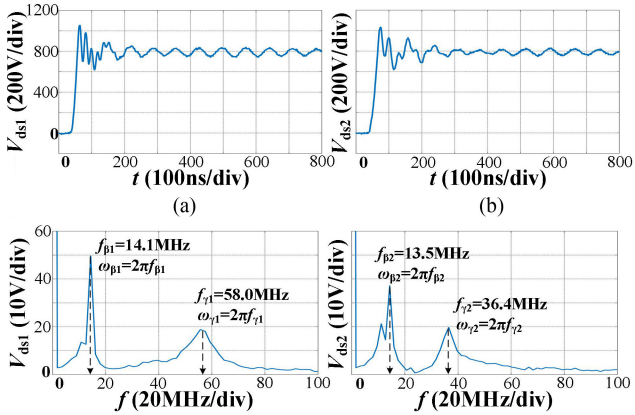

(a) (b) (c) (d)

Fig. 10. Experimental waveforms of V_{ds} in the laminated bus bar. (a) V_{ds1} without C_o. (b) V_{ds2} with C_o. (c) and (d) Frequency spectrum.

C. Extraction in Capacitance-Included Laminated Bus Bar

A laminated bus bar used in the wind power converter is tested, as shown in Fig. 9. The extraction path is selected from the dc link (dc+/dc−) to one power module (IGBT II). The V_b is selected as 800 V with 10 A I_{load} and C_o is selected as 220 pF.

Fig. 10(a) and (b) demonstrates the oscillation waveforms of V_{ds} in a laminated bus bar experiment. The $\omega_{\beta1}$, $\omega_{\gamma1}$, $\omega_{\beta2}$, and $\omega_{\gamma2}$ are extracted by the FFT analysis from $f_{\beta1}$, $f_{\gamma1}$, $f_{\beta2}$, and $f_{\gamma2}$ in Fig. 10(c) and (d). According to formula (5), the calculation results are presented in Table IV. The C_{oss} is calculated as 124 pF. It is close to the result from the datasheet of SiC MOSFET. It is proved that the stray inductance and capacitance in the laminated bus bar can be extracted with acceptable error.

TABLE IV
EXPERIMENTAL AND IMPEDANCE ANALYZER RESULT OF LAMINATED BUS BAR

Symbol	Experiment	Impedance analyzer	Relative error
L_{lam}	43.8 nH	44.4 nH	1.4 %
C_{lam}	2.76 nF	2.81 nF	1.7 %

IV. CONCLUSION

A stray parameters extraction method is proposed based on the frequency information in the turn-off procedure. The stray inductance and capacitance are calculated by solving a set of frequency-based equations derived from the equivalent circuit. The experimental results in the copper and laminated bus bars validate the feasibility of the method. Compared with the TDM, the proposed frequency-based method avoids the synchronization problem and voltage offset from the parasitic resistor. This method can also be extended to a standardized and fully automated stray parameter testing procedure for the large-capacity power converters.

REFERENCES

[1] L. Müller and J. W. Kimball, "Effects of stray inductance on hard-switched switched capacitor converters," *IEEE Trans. Power Electron.*, vol. 29, no. 12, pp. 6276–6280, Dec. 2014.

[2] Y. J. Ko, H. Jedtberg, G. Buticchi, and M. Liserre, "Analysis of DC-Link current influence on temperature variation of capacitor in a wind turbine application," *IEEE Trans. Power Electron.*, vol. 33, no. 4, pp. 3441–3451, Apr. 2018.

[3] Y. Jiang *et al.*, "An experimental method for extracting stray inductance of bus bars without high bandwidth current measurement," in *Proc. IEEE Energy Convers. Congr. Expo.*, Cincinnati, OH, USA, 2017, pp. 1446–1450.

[4] C. Chen, X. Pei, Y. Chen, and Y. Kang, "Investigation, evaluation, and optimization of stray inductance in laminated busbar," *IEEE Trans. Power Electron.*, vol. 29, no. 7, pp. 3679–3693, Jul. 2014.

[5] B. Lu *et al.*, "Determination of stray inductance of low-inductive laminated planar multiport busbars using vector synthesis method," *IEEE Trans. Ind. Electron.*, vol. 67, no. 2, pp. 1337–1347, Feb. 2020.

[6] S. Li, L. M. Tolbert, F. Wang, and F. Z. Peng, "Stray inductance reduction of commutation loop in the P-cell and N-cell-Based IGBT phase leg module," *IEEE Trans. Power Electron.*, vol. 29, no. 7, pp. 3616–3624, Jul. 2014.

[7] L. Yuan, Q. Gu, G. Feng, Z. Zhao, R. Yang, and W. Wang, "Experimental research on stray inductance extraction of planar bus bars based on HVIGBT dynamic characteristics," in *Proc. 17th Int. Conf. Elect. Mach. Syst.*, 2014, pp. 1957–1962.

[8] Y. Liu, Z. Zhao, W. Wang, and J.-S. Lai, "Characterization and extraction of power loop stray inductance with SiC half-bridge power module," *IEEE Trans. Electron. Devices*, vol. 67, no. 10, pp. 4040–4045, Oct. 2020.

[9] D.-P. Sadik, K. Kostov, J. Colmenares, F. Giezendanner, P. Ranstad, and H.-P. Nee, "Analysis of parasitic elements of SiC power modules with special emphasis on reliability issues," *IEEE J. Emerg. Sel. Topics Power Electron.*, vol. 4, no. 3, pp. 988–995, Sep. 2016.

[10] M. C. Caponet, F. Profumo, R. W. D. Doncker, and A. Tenconi, "Low stray inductance bus bar design and construction for good EMC performance in power electronic circuits," *IEEE Trans. Power Electron.*, vol. 17, no. 2, pp. 225–231, Mar. 2002.

[11] T. Liu, R. Ning, T. T. Y. Wong, and Z. J. Shen, "Modeling and analysis of SiC MOSFET switching oscillations," *IEEE J. Emerg. Sel. Topics Power Electron.*, vol. 4, no. 3, pp. 747–756, Sep. 2016.